

Chiral 2π -exchange NN-potentials: Relativistic $1/M^2$ -Corrections

N. Kaiser

Physik Department T39, Technische Universität München, D-85747 Garching, Germany

Abstract

We calculate in baryon chiral perturbation theory the relativistic $1/M^2$ -corrections to the leading order two-pion exchange diagrams. We give explicit expressions for the corresponding one-loop NN-amplitudes in momentum space. The resulting isovector central and isoscalar spin-spin and tensor NN-amplitudes involve non-static terms proportional to the squared nucleon center-of-mass momentum p^2 . From the two-pion exchange box diagrams we obtain an isoscalar quadratic spin-orbit NN-amplitude. We give also analytical expressions for the corresponding NN-potentials in coordinate space. The diagrammatic results presented here make the chiral NN-potential complete at next-to-next-to-next-to-leading order.

PACS: 12.20.Ds, 12.38.Bx, 12.39.Fe, 13.75.Cs.

Over the past years effective field theory methods have been successfully applied to the two-nucleon system at low and intermediate energies [1, 2, 3, 4, 5, 6]. The idea of constructing the NN-potential from effective field theory was put forward by Weinberg [1] and this was first taken up by van Kolck and collaborators [2] who used "old-fashioned" time-ordered perturbation theory. Later, the systematic method of unitary transformations was employed by Epelbaum, Glöckle and Meißner [4] to construct an energy-independent NN-potential from the effective chiral pion-nucleon Lagrangian at (next-to-)next-to-leading order. Based on one- and two-pion exchange and nine adjustable NN-contact interactions which contribute only to S- and P-waves a good description of the deuteron properties as well as the NN phase-shifts and mixing angles below $T_{\text{lab}} = 300$ MeV was found in that framework [4]. Also recently, the elastic proton-proton scattering database below 350 MeV laboratory kinetic energy (consisting of 1951 data points) has been analyzed in terms of 1π -exchange and chiral 2π -exchange at next-to-next-to-leading order in ref.[7]. The resulting good $\chi^2/\text{dof} \leq 1$ constitutes a convincing proof for the presence of the chiral 2π -exchange in the long-range proton-proton strong interaction. It was concluded in ref.[7] that 1π -exchange together with chiral 2π -exchange gives a very good NN-force at least as far inwards as $r = 1.4$ fm internucleon distance. All shorter range components of the NN-interaction have been effectively parametrized in ref.[7] by 23 boundary condition parameters.

At present, there is much interest in extending the calculations of the two-nucleon system [8] (and also the analysis of the NN database) to one order higher in the chiral expansion. This requires the full knowledge of the next-to-next-to-next-to-leading order ($N^3\text{LO}$) chiral NN-potential. In momentum space this corresponds to terms in the NN T-matrix which are of fourth order in small external momenta and the pion mass, denoted generically by $\mathcal{O}(Q^4)$. In particular, all two-loop diagrams of the process $NN \rightarrow NN$ with leading order vertices contribute at that order, $\mathcal{O}(Q^4)$. The chiral 3π -exchange has recently been calculated completely in ref.[9]. Furthermore, results for the two-loop 2π -exchange are now available from ref.[10]. In that work also the one-loop contributions (of order $\mathcal{O}(Q^4)$) proportional to the second and third order low-energy constants $c_{1,2,3,4}$ and \bar{d}_j , related to elastic πN -scattering, have been evaluated. The only remaining and presently unknown pieces of the NN T-matrix at order $\mathcal{O}(Q^4)$ are the relativistic $1/M^2$ -corrections to the leading order one-loop 2π -exchange. The purpose of this work is to present analytical results for these remaining contributions and thus to complete the chiral NN-potential at next-to-next-to-next-to-leading order.

Let us first give some basic definitions in order to fix our notation. We are considering elastic NN-scattering in the center-of-mass frame, i.e. the process $N_1(\vec{p}) + N_2(-\vec{p}) \rightarrow N_1(\vec{p} + \vec{q}) + N_2(-\vec{p} - \vec{q})$. The corresponding on-shell T-matrix has the following general form,

$$\begin{aligned} \mathcal{T}_{NN} = & V_C + \vec{\tau}_1 \cdot \vec{\tau}_2 W_C + [V_S + \vec{\tau}_1 \cdot \vec{\tau}_2 W_S] \vec{\sigma}_1 \cdot \vec{\sigma}_2 + [V_T + \vec{\tau}_1 \cdot \vec{\tau}_2 W_T] \vec{\sigma}_1 \cdot \vec{q} \vec{\sigma}_2 \cdot \vec{q} \\ & + [V_{SO} + \vec{\tau}_1 \cdot \vec{\tau}_2 W_{SO}] i(\vec{\sigma}_1 + \vec{\sigma}_2) \cdot (\vec{q} \times \vec{p}) \\ & + [V_Q + \vec{\tau}_1 \cdot \vec{\tau}_2 W_Q] \vec{\sigma}_1 \cdot (\vec{q} \times \vec{p}) \vec{\sigma}_2 \cdot (\vec{q} \times \vec{p}), \end{aligned} \quad (1)$$

with $q = |\vec{q}|$ the momentum transfer between the initial and final-state nucleon, subject to the constraint $2\vec{p} \cdot \vec{q} = -q^2$. The subscripts C, S, T, SO and Q refer to the central, spin-spin, tensor, spin-orbit and quadratic spin-orbit components, each of which occurs in an isoscalar ($V_{C,\dots,Q}$) and an isovector ($W_{C,\dots,Q}$) version. Furthermore, $\vec{\sigma}_{1,2}$ and $\vec{\tau}_{1,2}$ in eq.(1) denote the spin and isospin operators of the two nucleons.

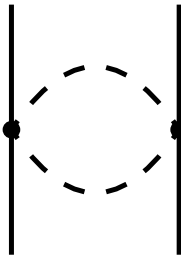


Fig.1: 2π -exchange bubble diagram. The combinatoric factor of this graph is $1/2$.

Let us now turn to the results for the $1/M^2$ -corrections to the chiral 2π -exchange. The bubble or football diagram involving two isovectorial Tomozawa-Weinberg vertices is shown in Fig. 1. A convenient way to obtain all $1/M^2$ -corrections from such a one-loop diagram goes as follows. At the left nucleon line one expands in the NN center-of-mass frame the pertinent relativistic $\pi\pi NN$ -vertex sandwiched between Dirac-spinors for the out- and in-going nucleon in powers of $1/M$ up to quadratic order, i.e. $\mathcal{O}(M^{-2})$. The analogous expression at the right nucleon line is obtained simply by switching the signs of three-momenta \vec{p} and \vec{q} and of the loop four-momentum (l_0, \vec{l}) . Of course, one also relabels the spin and isospin operators, $\vec{\sigma}_1 \rightarrow \vec{\sigma}_2$ and $\vec{\tau}_1 \rightarrow \vec{\tau}_2$. In a last step, one multiplies the product of these both expressions with the pion propagators and carries out the four-dimensional loop integration. The total result for the $1/M^2$ -corrections to the bubble diagram in Fig. 1 reads (displaying only non-vanishing contributions),

$$W_C = \frac{(q^2 - 4p^2)w^2 L(q)}{768\pi^2 M^2 f_\pi^4}, \quad (2)$$

$$W_{SO} = 3W_T = -\frac{3}{q^2}W_S = -\frac{w^2 L(q)}{512\pi^2 M^2 f_\pi^4}, \quad (3)$$

with the frequently occurring logarithmic loop function

$$L(q) = \frac{w}{q} \ln \frac{w+q}{2m_\pi}, \quad w = \sqrt{4m_\pi^2 + q^2}. \quad (4)$$

In eqs.(2,3) and in the following we omit purely polynomial terms which can be absorbed in the strength of some zero-range NN-contact interactions. In fact, we are interested here only in non-polynomial or finite-range terms from chiral 2π -exchange. Note also that the isovector central NN-amplitude W_C in eq.(2) has a non-static contribution proportional the squared nucleon center-of-mass momentum p^2 .

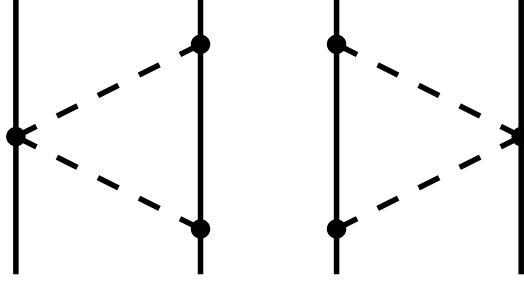


Fig.2: 2π -exchange triangle diagrams.

Fig. 2 shows the 2π -exchange triangle diagrams. The expression for the $\pi\pi NN$ -vertex at the left (or right) nucleon line of the first (second) diagram can be taken over from the calculation of the bubble diagram. At the other (right or left) nucleon line one expands in powers of $1/M$ the product of upper pseudovector πN -vertex, nucleon Dirac-propagator and lower pseudovector πN -vertex sandwiched between out- and in-going Dirac-spinors. Collecting all possible terms proportional to $1/M^2$ and performing the loop integration over the pion propagators, the total result for the $1/M^2$ -corrections to the triangle diagrams in Fig. 2 reads

$$W_C = \frac{g_A^2 L(q)}{96\pi^2 M^2 f_\pi^4} \left\{ \frac{11}{4} q^4 + 5m_\pi^2 q^2 + 3m_\pi^4 - 6m_\pi^6 w^{-2} - p^2(8m_\pi^2 + 5q^2) \right\}, \quad (5)$$

$$W_T = -\frac{1}{q^2} W_S = \frac{g_A^2 L(q)}{48\pi^2 M^2 f_\pi^4} \left\{ m_\pi^2 + \frac{7}{16} q^2 \right\}, \quad (6)$$

$$W_{SO} = \frac{g_A^2 L(q)}{32\pi^2 M^2 f_\pi^4} \left\{ m_\pi^2 + \frac{3}{8} q^2 \right\}. \quad (7)$$

Again, the isovector central NN-amplitude W_C in eq.(5) has a non-static piece proportional to p^2 . In the heavy nucleon mass limit $M \rightarrow \infty$ the diagrams in Fig. 1 and Fig. 2 give rise only to a non-vanishing isovector central NN-amplitude W_C (see eq.(14) in ref.[5]) and one finds that the non-static p^2 -terms in eqs.(2,5) are in fact proportional to it.

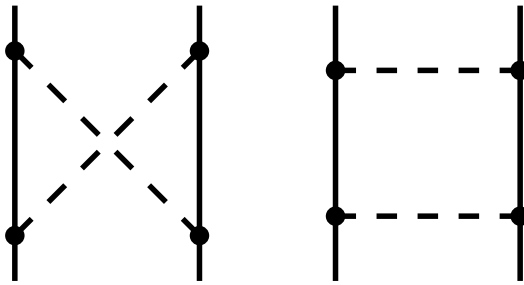


Fig.3: 2π -exchange box diagrams. The (right) planar box graph includes the iterated 1π -exchange.

Fig. 3 shows the 2π -exchange crossed box and planar box diagrams. The crossed box diagram (of isospin structure $3 + 2\vec{\tau}_1 \cdot \vec{\tau}_2$) can be evaluated straightforwardly by making use of the expression for the sequential pion absorption and emission process derived in the calculation of the triangle diagrams. At the left and the right nucleon line these expressions differ just by the sign of the three-momenta \vec{p} and \vec{q} . The planar box diagram (of isospin structure $3 - 2\vec{\tau}_1 \cdot \vec{\tau}_2$) requires some special treatment since it contains the so-called iterated 1π -exchange. As outlined in section 4.2 of ref.[5] one must perform the dl_0 loop integration (using e.g. residue calculus) before the $1/M$ -expansion in order to isolate the iterated 1π -exchange together with its own relativistic $1/M$ -corrections. From that (and also from a consideration of the Lorentz-invariant

NN two-body phase space) one finds a dependence of the iterated 1π -exchange on the nucleon mass M of the form $M^2/\sqrt{M^2+p^2} = M - p^2/2M + \mathcal{O}(M^{-3})$. Since there obviously is no contribution to the iterated 1π -exchange proportional to $1/M^2$ one can treat (for the present purpose) the planar box graph in the same way as the crossed box graph. Namely, one performs first the $1/M$ -expansion of vertices and propagators at the left and the right nucleon line and then one carries out the four-dimensional loop integration. We have used this method as well as the continuation of the method outlined in section 4.2 of ref.[5] (where things are basically done in the reverse order) in order to calculate the $1/M^2$ -corrections to the planar box graph and we have found perfect agreement. Sorting finally the contributions from the crossed box diagram and planar box diagram in Fig. 3 into isoscalar and isovector components, we find after a tedious calculation

$$V_C = \frac{g_A^4}{32\pi^2 M^2 f_\pi^4} \left\{ \frac{1}{2} m_\pi^6 w^{-2} + \left[2m_\pi^8 w^{-4} + 8m_\pi^6 w^{-2} - q^4 - 2m_\pi^4 \right] L(q) \right\}, \quad (8)$$

$$W_C = \frac{g_A^4}{192\pi^2 M^2 f_\pi^4} \left\{ 4m_\pi^6 w^{-2} + \left[p^2 (20m_\pi^2 + 7q^2 - 16m_\pi^4 w^{-2}) + 16m_\pi^8 w^{-4} + 12m_\pi^6 w^{-2} - \frac{27}{4} q^4 - 11m_\pi^2 q^2 - 6m_\pi^4 \right] L(q) \right\}, \quad (9)$$

$$V_T = -\frac{1}{q^2} V_S = -\frac{g_A^4 L(q)}{32\pi^2 M^2 f_\pi^4} \left\{ p^2 + \frac{3}{8} q^2 + m_\pi^4 w^{-2} \right\}, \quad (10)$$

$$W_T = -\frac{1}{q^2} W_S = -\frac{g_A^4 L(q)}{384\pi^2 M^2 f_\pi^4} \left\{ 7m_\pi^2 + \frac{17}{4} q^2 + 4m_\pi^4 w^{-2} \right\}, \quad (11)$$

$$V_{SO} = \frac{g_A^4 L(q)}{8\pi^2 M^2 f_\pi^4} \left\{ \frac{11}{32} q^2 + m_\pi^4 w^{-2} \right\}, \quad (12)$$

$$W_{SO} = \frac{g_A^4 L(q)}{384\pi^2 M^2 f_\pi^4} \left\{ 4m_\pi^4 w^{-2} - \frac{11}{4} q^2 - 9m_\pi^2 \right\}, \quad (13)$$

$$V_Q = -\frac{g_A^4 L(q)}{32\pi^2 M^2 f_\pi^4}. \quad (14)$$

Here, one observes that the isovector central NN-amplitude W_C and the isoscalar spin-spin and tensor NN-amplitudes $V_{S,T}$ in eqs.(9,10) receive non-static contributions proportional to p^2 . Another interesting feature is the occurrence of an isoscalar quadratic spin-orbit NN-amplitude V_Q in eq.(14), whereas the analogous isovector NN-amplitude vanishes, $W_Q = 0$. This completes the presentation of analytical results for the momentum space NN-amplitudes.

For certain applications [7] it is useful to have a representation of the NN-interaction in terms of local coordinate space potentials. These potentials are related to the momentum space NN-amplitudes by a negative Fourier-transform, $-(2\pi)^{-3} \int d^3q \exp(i\vec{q}\cdot\vec{r})$. The isoscalar central, spin-spin, tensor and spin-orbit potentials, denoted here by $\tilde{V}_{C,S,T,SO}(r)$, are accompanied by the operators 1 , $\vec{\sigma}_1 \cdot \vec{\sigma}_2$, $3\vec{\sigma}_1 \cdot \hat{r} \vec{\sigma}_2 \cdot \hat{r} - \vec{\sigma}_1 \cdot \vec{\sigma}_2$ and $-\frac{i}{2}(\vec{\sigma}_1 + \vec{\sigma}_2) \cdot (\vec{r} \times \vec{\nabla})$. In the case of the isovector potentials $\tilde{W}_{C,S,T,SO}(r)$ an additional isospin operator $\vec{\tau}_1 \cdot \vec{\tau}_2$ occurs. The finite-range parts (disregarding zero-range $\delta^3(\vec{r})$ -terms) of the coordinate space potentials following from eqs.(2-14) are most conveniently obtained through their spectral-representations [9, 10] with the help of the formula $\text{Im } L(i\mu) = -(\pi/2\mu)\sqrt{\mu^2 - 4m_\pi^2}$. It turns out that all these potentials can be written analytically in terms of two modified Bessel-functions $K_{0,1}(2x)$, with the dimensionless variable $x = m_\pi r$. We list them separately for the three classes of diagrams.

i) Bubble diagram in Fig. 1:

$$\tilde{W}_C(r) = \frac{m_\pi}{128\pi^3 M^2 f_\pi^4 r^6} \left\{ 2x(5 + x^2 + p^2 r^2) K_0(2x) + (10 + 7x^2 + 2p^2 r^2) K_1(2x) \right\}, \quad (15)$$

$$\widetilde{W}_S(r) = \frac{m_\pi}{384\pi^3 M^2 f_\pi^4 r^6} \left\{ 2x(5+x^2)K_0(2x) + (10+7x^2)K_1(2x) \right\}, \quad (16)$$

$$\widetilde{W}_T(r) = -\frac{m_\pi}{1536\pi^3 M^2 f_\pi^4 r^6} \left\{ x(35+4x^2)K_0(2x) + (35+20x^2)K_1(2x) \right\}, \quad (17)$$

$$\widetilde{W}_{SO}(r) = -\frac{3m_\pi}{256\pi^3 M^2 f_\pi^4 r^6} \left\{ 5xK_0(2x) + (5+2x^2)K_1(2x) \right\}. \quad (18)$$

ii) Triangle diagrams in Fig. 2:

$$\begin{aligned} \widetilde{W}_C(r) &= \frac{g_A^2 m_\pi}{64\pi^3 M^2 f_\pi^4 r^6} \left\{ x(110+34x^2+x^4+p^2 r^2)K_0(2x) \right. \\ &\quad \left. + [110+89x^2+9x^4+(10+4x^2)p^2 r^2]K_1(2x) \right\}, \end{aligned} \quad (19)$$

$$\widetilde{W}_S(r) = -\frac{g_A^2 m_\pi}{192\pi^3 M^2 f_\pi^4 r^6} \left\{ 10x(7+2x^2)K_0(2x) + (70+55x^2+4x^4)K_1(2x) \right\}, \quad (20)$$

$$\widetilde{W}_T(r) = \frac{g_A^2 m_\pi}{768\pi^3 M^2 f_\pi^4 r^6} \left\{ x(245+52x^2)K_0(2x) + (245+170x^2+8x^4)K_1(2x) \right\}, \quad (21)$$

$$\widetilde{W}_{SO}(r) = \frac{g_A^2 m_\pi}{128\pi^3 M^2 f_\pi^4 r^6} \left\{ x(45+4x^2)K_0(2x) + (45+24x^2)K_1(2x) \right\}. \quad (22)$$

iii) Box diagrams in Fig. 3:

$$\widetilde{V}_C(r) = -\frac{g_A^4 m_\pi}{16\pi^3 M^2 f_\pi^4 r^6} \left\{ x(30+12x^2+x^4)K_0(2x) + \left(30+27x^2+\frac{9}{2}x^4+\frac{x^6}{8} \right) K_1(2x) \right\}, \quad (23)$$

$$\begin{aligned} \widetilde{W}_C(r) &= \frac{g_A^4 m_\pi}{384\pi^3 M^2 f_\pi^4 r^6} \left\{ x[p^2 r^2(8x^2-42)-810-258x^2-6x^4]K_0(2x) \right. \\ &\quad \left. - [810+663x^2+70x^4+4x^6+p^2 r^2(42+8x^2)]K_1(2x) \right\}, \end{aligned} \quad (24)$$

$$\begin{aligned} \widetilde{V}_S(r) &= \frac{g_A^4 m_\pi}{192\pi^3 M^2 f_\pi^4 r^6} \left\{ x(90+36x^2+4x^4-12p^2 r^2)K_0(2x) \right. \\ &\quad \left. + [90+81x^2+14x^4-p^2 r^2(12+8x^2)]K_1(2x) \right\}, \end{aligned} \quad (25)$$

$$\widetilde{W}_S(r) = \frac{g_A^4 m_\pi}{1152\pi^3 M^2 f_\pi^4 r^6} \left\{ x(510+162x^2+8x^4)K_0(2x) + (510+417x^2+44x^4)K_1(2x) \right\}, \quad (26)$$

$$\begin{aligned} \widetilde{V}_T(r) &= \frac{g_A^4 m_\pi}{768\pi^3 M^2 f_\pi^4 r^6} \left\{ x(48p^2 r^2-315-114x^2-8x^4)K_0(2x) \right. \\ &\quad \left. + [p^2 r^2(60+16x^2)-315-270x^2-40x^4]K_1(2x) \right\}, \end{aligned} \quad (27)$$

$$\widetilde{W}_T(r) = -\frac{g_A^4 m_\pi}{4608\pi^3 M^2 f_\pi^4 r^6} \left\{ x(1785+456x^2+16x^4)K_0(2x) + (1785+1320x^2+112x^4)K_1(2x) \right\}, \quad (28)$$

$$\widetilde{V}_{SO}(r) = \frac{g_A^4 m_\pi}{128\pi^3 M^2 f_\pi^4 r^6} \left\{ x(165+52x^2)K_0(2x) + (165+132x^2+16x^4)K_1(2x) \right\}, \quad (29)$$

$$\widetilde{W}_{SO}(r) = \frac{g_A^4 m_\pi}{768\pi^3 M^2 f_\pi^4 r^6} \left\{ -x(165+4x^2)K_0(2x) + (8x^4-78x^2-165)K_1(2x) \right\}, \quad (30)$$

$$\tilde{V}_Q(r) = \frac{g_A^4 m_\pi}{64\pi^3 M^2 f_\pi^4 r^6} \left\{ 12x K_0(2x) + (15 + 4x^2) K_1(2x) \right\}, \quad (31)$$

The last potential $\tilde{V}_Q(r)$ is accompanied by the quadratic spin-orbit operator $-\vec{\sigma}_1 \cdot (\vec{r} \times \vec{\nabla}) \vec{\sigma}_2 \cdot (\vec{r} \times \vec{\nabla})$. In order to Fourier-transform the $w^{-4}L(q)$ -terms in eqs.(8,9) it is useful to exploit the relation $4m_\pi^2 w^{-4}L(q) + w^{-2} = -m_\pi(\partial/\partial m_\pi)[w^{-2}L(q)]$.

In Table 1, we present numerical values for the coordinate space potentials eqs.(15-31) at $p = 0$, using the parameters $g_A = 1.3$, $m_\pi = 138$ MeV, $f_\pi = 92.4$ MeV and $M = 939$ MeV. One observes that the attractive central potentials, $\tilde{V}_C(r)$ and $\tilde{W}_C(r)$, and the repulsive isoscalar spin-orbit potential $\tilde{V}_{SO}(r)$ are quite sizeable. The inclusion of the relativistic $1/M^2$ -corrections to the chiral 2π -exchange in NN phase-shift calculations etc. may therefore not be just a small effect. Of course, a firm conclusion about their relevance can only be drawn from the complete N³LO chiral NN-potential.

In summary, we have completed here the chiral NN-potential at next-to-next-to-next-to-leading order by evaluating the relativistic $1/M^2$ -corrections to 2π -exchange. The analytical results presented here are in a form such that they can be easily implemented in a N³LO calculation of the two-nucleon system or in an empirical analysis of low-energy elastic NN-scattering. Work along this line is in progress [8]. With such calculations one will be able to determine the maximal range of validity of chiral multi-pion exchange in the NN-interaction.

r [fm]	0.7	0.8	0.9	1.0	1.1	1.2	1.3	1.4
\tilde{V}_C [MeV]	-185.5	-72.3	-31.4	-14.9	-7.56	-4.06	-2.29	-1.34
\tilde{W}_C [MeV]	-103.7	-40.2	-17.4	-8.18	-4.13	-2.20	-0.28	-0.72
\tilde{V}_S [MeV]	46.4	18.1	7.86	3.73	1.89	1.02	0.57	0.34
\tilde{W}_S [MeV]	23.1	8.95	3.87	1.83	0.92	0.49	0.28	0.16
\tilde{V}_T [MeV]	-40.2	-15.6	-6.77	-3.20	-1.62	-0.87	-0.49	-0.29
\tilde{W}_T [MeV]	-19.9	-7.69	-3.32	-1.56	-0.78	-0.42	-0.23	-0.13
\tilde{V}_{SO} [MeV]	124.8	48.3	20.9	9.81	4.94	2.63	1.47	0.85
\tilde{W}_{SO} [MeV]	-2.15	-0.78	-0.31	-0.13	-0.06	-0.028	-0.013	-0.006
\tilde{V}_Q [MeV]	19.4	7.26	3.02	1.37	0.66	0.34	0.18	0.10

Tab.1: Numerical values of the relativistic $1/M^2$ -corrections to the chiral 2π -exchange NN-potentials (at $p = 0$) versus the nucleon distance r . The units of these potentials are MeV.

References

- [1] S. Weinberg, *Nucl. Phys.* **B363**, 3 (1991).
- [2] C. Ordonez, L. Ray and U. van Kolck, *Phys. Rev.* **C53**, 2086 (1996).
- [3] D.B. Kaplan, M.J. Savage and M.B. Wise, *Nucl. Phys.* **B534**, 329 (1998).
- [4] E. Epelbaum, W. Glöckle and Ulf-G. Meißner, *Nucl. Phys.* **A637**, 107 (1998); **A671**, 295 (2000); and references therein.
- [5] N. Kaiser, R. Brockmann and W. Weise, *Nucl. Phys.* **A625**, 758 (1997).
- [6] N. Kaiser, S. Gerstendörfer and W. Weise, *Nucl. Phys.* **A637**, 395 (1998).
- [7] M.C.M. Rentmeester, R.G.E. Timmermans, J.L. Friar and J.J. de Swart, *Phys. Rev. Lett.* **82**, 4992 (1999).
- [8] R. Machleidt, D. Phillips and R. Timmermans, private communications.
- [9] N. Kaiser, *Phys. Rev.* **C61** 014003 (2000); **C62** 024001 (2000); **C63** 044010 (2001).
- [10] N. Kaiser, *Phys. Rev.* **C64**, 0570XX (2001); nucl-th/0107064.